Engineering 7 (2021) 832–844

Contents lists available at ScienceDirect

Engineering

journal homepage: www.elsevier.com/locate/eng

Research
Medical Additive Manufacturing—Review

Bioprinting of Small-Diameter Blood Vessels

Xia Cao [#], Sushila Maharjan [#], Ramla Ashfaq, Jane Shin, Yu Shrike Zhang [*]

Division of Engineering in Medicine, Department of Medicine, Brigham and Women's Hospital, Harvard Medical School, Cambridge, MA 02139, USA

ARTICLE INFO

Article history:
Received 3 August 2019
Revised 15 February 2020
Accepted 6 March 2020
Available online 30 September 2020

Keywords:
Bioprinting
Small-diameter blood vessel
Bioink
Vascular engineering

ABSTRACT

There has been an increasing demand for bioengineered blood vessels for utilization in both regenerative medicine and drug screening. However, the availability of a true bioengineered vascular graft remains limited. Three-dimensional (3D) bioprinting presents a potential approach for fabricating blood vessels or vascularized tissue constructs of various architectures and sizes for transplantation and regeneration. In this review, we summarize the basic biology of different blood vessels, as well as 3D bioprinting approaches and bioink designs that have been applied to fabricate vascular and vascularized tissue constructs, with a focus on small-diameter blood vessels.

1. Introduction

Blood vessels are the conduits that transport oxygen and nutrients to the tissues and carry carbon dioxide and wastes from them. Arteries, capillaries, and veins are three main types of blood vessels, which differ in structural composition, dimension, and physiological function [1]. Based on the inner diameter (ID), blood vessels are broadly categorized into microvessels, having an ID less than 1 mm, small vessels, having an ID ranging from 1 to 6 mm, and large vessels, with an ID greater than 6 mm [2,3].

The aorta is the largest blood vessel in the human body; it transports oxygenated blood from the heart to different parts of the body. The aorta branches into arteries, which further divide into smaller vessels known as arterioles. The arterioles eventually branch into tiny capillaries; these are the smallest blood vessels, which allow the diffusion of oxygen, nutrients, carbon dioxide, and other metabolic wastes between the blood and the local tissues [4,5]. Capillaries form a network between the arterioles and venules, the latter of which are very small veins that collect deoxygenated blood from the capillaries and transport it into progressively larger veins until it re-enters the heart [6].

Although arteries and veins have different functions, their walls similarly consist of variable compositions of cells and extracellular matrix (ECM), which are grouped into three main layers: the innermost tunica intima, the middle tunica media, and the outer tunica adventitia (Fig. 1(a)) [7,8]. Capillaries (ID < 10 μm) consist of a single layer of endothelial cells (ECs) forming the inner lining of the blood vessel (tunica intima), and are surrounded by basal lamina and pericytes (Fig. 1(b)) [9,10]. Both arterioles and venules (ID = 10–100 μm) consist of an inner EC layer (tunica intima) with a surrounding thin smooth muscle cell (SMC) layer (tunica media) (Fig. 1(b)). Arteries and veins (ID > 100 μm) consist of an inner EC lining (tunica intima), a middle dense SMC layer (tunica media), and an outer layer of fibroblasts and ECM components (tunica adventitia) (Fig. 1(b)) [10,11]. Different layers of blood vessels with their cell composition, diameter, ECM components, and functions are listed in Table 1 [12,13].

ECs and vascular SMCs are the key cellular components of both arteries and veins. The interactions of these cell types play a critical role not only in the development of the vasculature, but also in maintaining vascular homeostasis [14]. The EC linings of blood vessels are significantly heterogeneous in phenotype and function, due to the varying microenvironments and different levels of pressures and shear stresses that they experience during blood flow [15]. The EC linings serve as tightly regulated dynamic barriers, preventing blood leakage into the surrounding tissue and interstitial space. They also play pivotal roles in several physiological processes, including regulation of blood flow and permeability, transendothelial migration of circulating immune cells at the site of inflammation, and maintenance of vascular tone and hemostasis [16,17]. While ECs are aligned longitudinally, SMCs are circumferentially aligned and interspaced by elastic fibers. SMCs possess the contractile phenotype and maintain vascular homeostasis through active contraction and relaxation. In addition, SMCs possess a

* Corresponding author.
E-mail address: yszhang@research.bwh.harvard.edu (Y.S. Zhang).
[#] These authors contributed equally to this work.

https://doi.org/10.1016/j.eng.2020.03.019

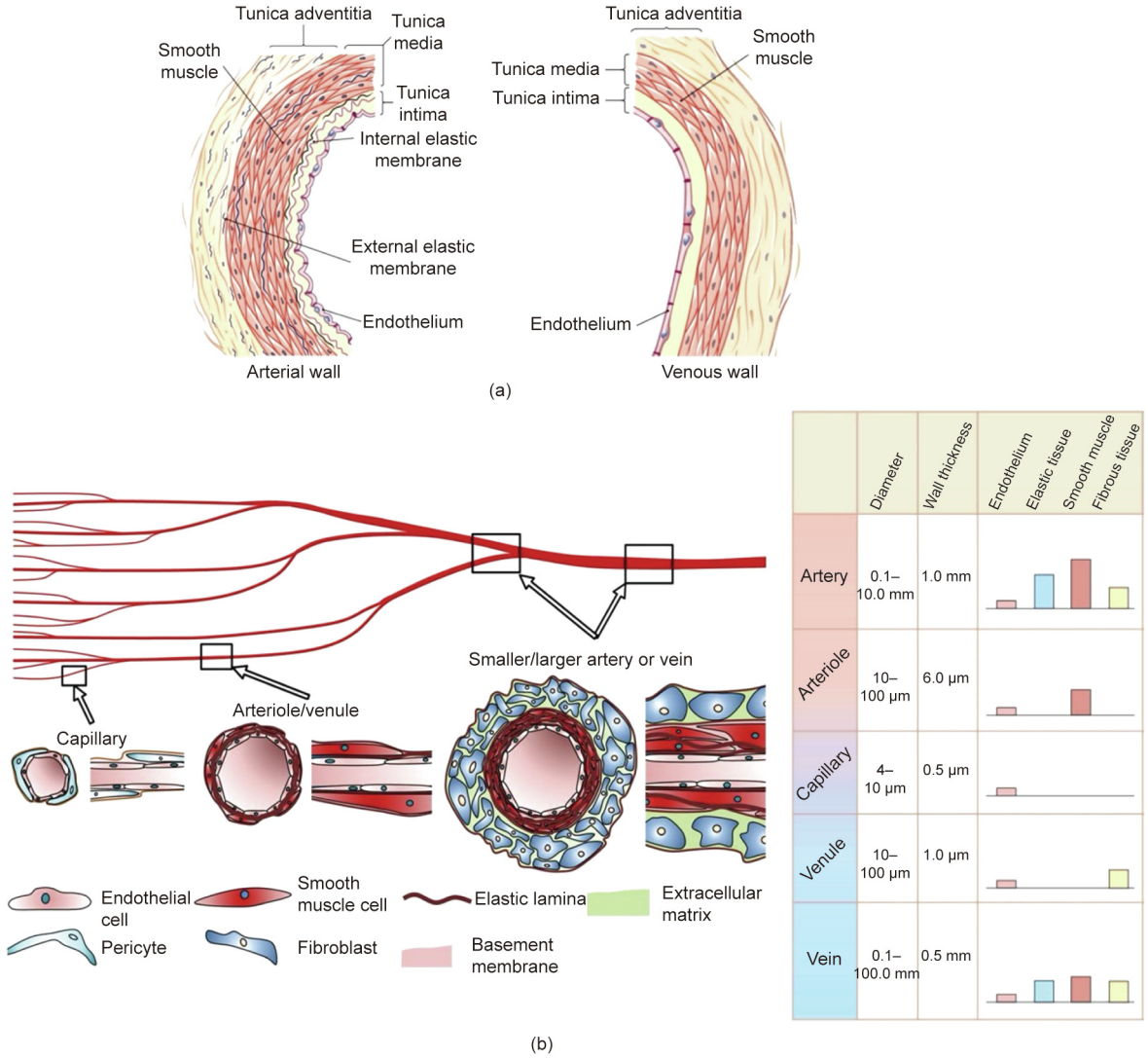

Fig. 1. The general structure and types of blood vessels. (a) Schematics of different layers of an arterial and venous wall. Reproduced from Ref. [8] with permission of Mary Hammes, © 2015. (b) Schematics of different types of blood vessels showing cell composition, diameters, and thickness. The bar in the table represents the relative proportion of different layers of blood vessel. A capillary comprises an EC lining surrounded by pericytes. An arteriole/venule consists of an EC lining surrounded by a thin layer of smooth muscle cells (SMCs). An artery/vein consists of an EC lining surrounded by a dense SMC layer and fibroblasts. Reproduced from Ref. [10] with permission of Nature, © 2018; and Ref. [11] with permission of the American Physiological Society, Inc., © 1954.

Table 1
The general structures and functions of blood vessels [12,13].

Blood vessel	Wall layer	Feature	Cell	ECM component	Function
Arteries/ veins	Tunica adventitia	Outermost layer, thicker in veins	Fibroblasts	Elastin, collagen types I and IV, and versican	Plays an important role in cell trafficking, immune response mediation, and vascular remodeling
	Tunica media	Middle layer, much thicker in arteries than in veins	SMCs and pericytes	Elastin; fibrillar collagen types I, III, and V; laminin; fibronectin; and proteoglycan	Regulates blood flow and pressure by controlling vasoconstriction and vasodilation of vessels
	Tunica intima	Innermost and thinnest layer	ECs	Laminin, fibronectin, collagen type IV, and nidogens	Provides structural integrity of the blood vessel by forming semipermeable membrane and thermoresistant wall; also controls blood flow and vessel tone
Capillaries	Tunica intima	Extremely thin single layer	ECs	Laminin, fibronectin, collagen type IV, and proteoglycan	Provides a semipermeable membrane for diffusion of oxygen, nutrients, carbon dioxide, and metabolic wastes between the blood and local tissue environment

secretory phenotype, which is responsible for the synthesis and repair of ECMs and thus regulates the structure of the vascular wall [18].

Coronary heart disease and peripheral arterial disease represent the leading causes of mortality and morbidity globally, with an annual mortality incidence estimated to increase to 23.3 million by 2030 [19]. Angioplasty, stent implantation, and surgical bypass grafting are the current commonly used revascularization approaches [20]. The use of autologous arteries or veins, mostly the internal thoracic artery or saphenous vein, remains the gold standard for bypass grafts for the treatment of vascular diseases such as coronary artery and peripheral vascular diseases [20]. However, healthy autologous vessels are not always available,

require invasive harvesting, and have poor long-term patency rates [21,22]. Synthetic vascular grafts, which are mostly made from polyethylene terephthalate or polytetrafluoroethylene, have been used as alternatives to autologous vessels for the successful replacement of medium and large vessels [23,24]. Although these synthetic grafts have proven effective for medium and large vessels with long-term patency, their adoption has been limited for small vessels due to mismatched biomechanical properties, poor biocompatibility, thrombogenicity, microbiological contamination, and poor patency rates [25–27]. Considering the limitations of current vascular conduits and the pathological events in small-diameter blood vessels including coronary arteries and peripheral arteries, there is a persistent clinical demand for bioengineered vascular conduits with the potential to reduce the morbidity associated with small-diameter vascular disease [28].

With the progress that has been achieved in vascular bioengineering, three-dimensional (3D) bioprinting has emerged as a potential approach for generating blood vessels with the ability to grow, remodel, and repair vascular disease *in vivo*. Different 3D bioprinting techniques and strategies have been investigated and established over the past years to fabricate biomimetic blood vessels and are constantly being refined and improved [29–32]. In this review article, we summarize different bioprinting techniques, including extrusion bioprinting, inkjet bioprinting, laser-assisted bioprinting, and vat polymerization-based bioprinting, applied to the engineering of small-diameter blood vessels, including small vessels and microvessels, along with their strengths and limitations. We also discuss different biomaterials and their properties relating to biocompatibility, printability, and mechanical properties, as well as the challenges involved in the formulation of appropriate bioinks that satisfy the critical requirements for the 3D bioprinting of small-diameter blood vessels. We conclude with potential future directions.

2. 3D bioprinting

3D bioprinting has significantly advanced in the field of vascular tissue engineering. The essential requirements for engineering blood vessels with long-term patency include appropriate mechanical properties, high compliance, remodeling capability, and anti-thrombogenicity, in order to achieve successful integration with the native blood vessels [33]. The requirements for ideal bioengineered vessels—particularly small-diameter blood vessels—are listed in Table 2 [25]. 3D bioprinting permits the precise deposition of biomaterials and living cells (together termed as "bioink") in well-defined spatial patterns that closely mimic the structures of blood vessels [34]. Vascular tissue engineering through bioprinting has been accomplished via various modalities and strategies, along with a wide range of bioinks [24]. The most commonly used bioprinting modalities include inkjet [35], extrusion [36,37], laser-assisted [38], and vat polymerization-based bioprinting [39,40]. The inkjet method, which is a non-contact bioprinting technique, deposits bioink droplets of a predetermined size from a cartridge to generate pseudo-3D or 3D structures (Fig. 2(a)) [31,41]. Extrusion bioprinting is the most commonly used bioprinting method, in which the bioink is dispensed continuously in the form of filaments through a nozzle (Fig. 2(b)) [31,42]. Laser-assisted bioprinting is comparatively less common than inkjet and extrusion and uses laser pulses to deposit the bioink from the donor slide onto the receiver substrate (Fig. 2(c)) [31,43,44]. Vat polymerization-based bioprinting, typically in the form of stereolithography or digital light processing, uses precisely controlled patterns of light to polymerize photosensitive polymers on a vertically movable platform to create 3D constructs with desired architectures (Fig. 2(d)) [45,46].

Each modality has its strengths and limitations and differs in several parameters such as choice of bioinks and substrates utilized, complexity of patterns, and yield of fabrication [47]. Inkjet bioprinting offers several advantages including rapid bioink deposition and high resolution; however, it often has limited capacity due to instability of the dispensed layers [48,49]. Extrusion bioprinting is a cost-effective method with ease of control. However, it is a comparatively slow method and has lower resolution [50]. Laser-assisted bioprinting provides rapid fabrication, high resolution, and biocompatibility but at high instrument cost [51]. Vat polymerization-based bioprinting also offers high resolution and rapid fabrication, with instrumentation of medium complexity [52]. Depending on the varying shapes and sizes of blood vessels, different 3D bioprinting modalities have been applied to fabricate vasculature with varied degrees of function *in vitro* (Fig. 2(e)) [5].

Table 2
Requirements for an ideal bioengineered small-diameter blood vessel. Reproduced from Ref. [25] with permission of Valentina Catto et al., © 2014.

Description	Requirement
Biocompatibility	Nontoxicity Nonimmunogenicity Nonthrombogenicity Nonsusceptibility to infection Maintenance of a functional endothelium
Mechanical properties	Compliance similar to native vessel Burst pressure similar to native vessel Kink and compression resistance Good suture retention
Processability	Low manufacturing costs Sterile or sterilizable Easy storage Readily available with a variety of lengths and diameters

3. Bioink designs

To be functional, the structure and integrity of bioengineered vasculature must resemble those of native blood vessels, both of which are highly dependent on mechanical and chemical cues from the surrounding ECM [53]. The ECM serves as a reservoir and modulator for various cytokines and growth factors, as well as providing structural support for EC organization and stabilization during blood vessel formation [54]. Thus, ECM properties such as density, heterogeneity, and stiffness play critical roles in regulating vascular morphogenesis, capillary network formation, and barrier integrity [55,56].

The major ECM components that comprise different layers of blood vessels are shown in Table 1 [12,13]. Vessel lumens are lined with ECs, resting on a basement membrane that is largely composed of collagens, laminins, fibronectin, nidogen, heparin sulfate proteoglycans, entactin, and other macromolecules [54,57]. Tunica media, the middle SMC layer, is composed of collagenous ECM containing fibrillar collagens I, III, and V; laminin; elastin; fibronectin; hyaluronan; and decorin [58–60]. Tunica intima and tunica media are separated by the internal elastic lamina. The tunica adventitia, the outermost layer of connective tissue and fibroblasts, consists of elastin, collagen types I and IV, and versican. Tunica media and tunica adventitia are separated by the external elastic lamina [57,59–61].

To this end, the successful *in vitro* fabrication of blood vessels, particularly those with small diameters, requires synergy between higher-resolution bioprinting approaches and adequate bioink formulations that can provide structural and mechanical support to maintain cell viability while facilitating grafting or neovascularization [62]. A bioink is a combination of biomaterial(s), cells, nutrients, and/or growth factors that should mimic the optimal ECM environment of the tissue [63]. The design of a bioink should consider major ECM components, and is critical for the 3D bioprinting of vessels as it determines not only the bioprinting

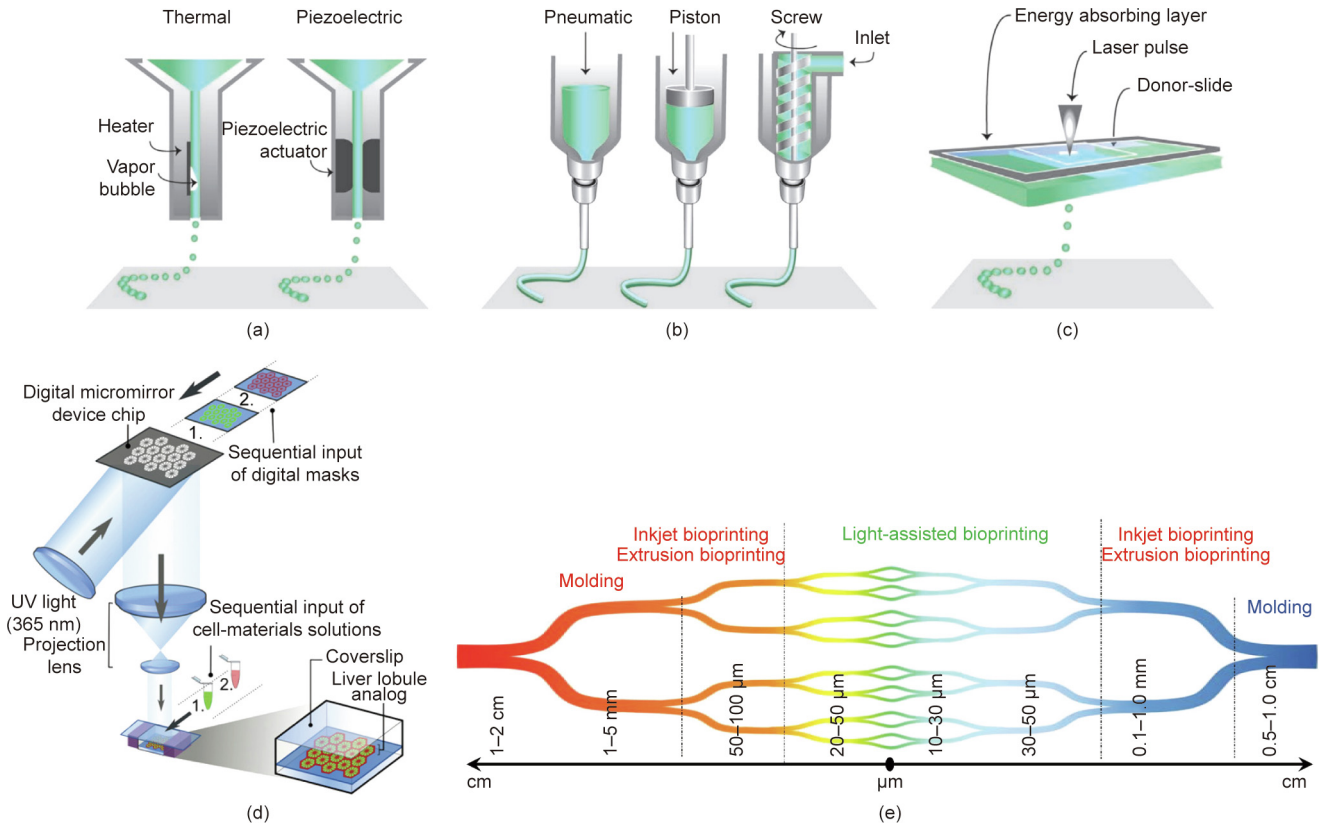

Fig. 2. Representative 3D bioprinting approaches. (a) Schematic of inkjet bioprinting method. (b) Schematic of extrusion bioprinting method. (c) Schematic of laser-assisted bioprinting method. (a–c) are reproduced from Ref. [44] with permission of Wiley, © 2013. (d) Schematic of vat polymerization-based bioprinting method. Reproduced from Ref. [46] with permission of Xuanyi Ma et al., © 2016. (e) Schematic showing the hierarchy of blood vessels and the current bioprinting techniques that have been employed to fabricate the range of different blood vessels. Reproduced from Ref. [5] with permission of Elsevier, © 2019.

resolution but also vessel integrity and other critical biological properties [64–66].

The most popular formulation of bioink for 3D bioprinting of blood vessels is based on hydrogel precursors, due to their excellent biocompatibility, tunable stiffness and porosity, and ability to mimic native ECM, as well as their compatibility with different bioprinting modalities [67]. Several natural and synthetic biomaterials have been investigated, alone or in combination, for designing bioink that resembles the physicochemical properties of the ECM. Natural biomaterials that have been widely used for *in vitro* vascular tissue engineering include gelatin [68–71], collagen [72–77], elastin [78–81], fibrin [82–85], hyaluronic acid [68,86,87], agarose [49,88], alginate [89,90], and Matrigel [91–93], among others. Natural biomaterial-based hydrogel provides a suitable microenvironment for cell adhesion, growth, and proliferation; most importantly, it does not typically cause chronic inflammation or toxicity to the host [74]. However, the weak mechanical strength of naturally derived hydrogels fails to withstand physiological pressure and thus limits their usage in vascular tissue engineering [94]. Therefore, various synthetic polymers have been investigated, in combination with natural biomaterials, for such applications because of their precisely controlled mechanical properties, porosity, reproducibility, structural diversity, stiffness, and biodegradation [95]. Commonly used synthetic polymers include poly(ethylene glycol) (PEG) [96,97], poly(hydroxyethyl methacrylate) [98], and poly(vinyl alcohol) (PVA) [99,100]. These composite materials can provide good mechanical support and increase the mechanical strength of printed structures. However, the application of synthetic polymers is limited due to their lack of biocompatibility, poor cell adhesion, release of toxic byproducts, and decrease in mechanical properties due to the degradation process [47].

To overcome these limitations and obtain bioinks with desirable properties, functionalization has been explored using different methods based on chemical, mechanical, physical, and biological modifications. One of the most commonly adopted functionalization methods is the introduction of methacryloyl groups to polymers such as gelatin [101–105], collagen [106,107], and hyaluronic acid [108,109]. This method results in photopolymerizable polymers that can form mechanically stable constructs when needed. The mechanical strength of these polymers depends largely on the degree of methacryloyl modification and light exposure, with higher degree of methacryloyl modification and longer light exposure leading to increased stiffness of the constructs and decreased degradation [110]. The application of two or more crosslinking mechanisms contributes significantly to increased structural integrity and mechanical strength [110,111]. For example, improved mechanical properties were achieved when a decellularized ECM (dECM) bioink was covalently crosslinked using vitamin B2 (riboflavin) [112], followed by thermally triggered physical crosslinking via collagen fibrillogenesis [113]. This two-step crosslinking mechanism demonstrated a superior storage modulus compared with constructs crosslinked separately, indicating that each crosslinking mechanism contributes to the overall

mechanical properties of the constructs [113]. On the other hand, combining bioink materials may achieve the same phenomenon. For example, the addition of gelatin to gelatin methacryloyl (GelMA) increased the degree of crosslinking and thus the mechanical properties [114]. In addition, when other polymers, such as methylcellulose [115], 4-arm PEG-tetra-acrylate (PEGTA) [110], 8-arm PEG-acrylate with a tripentaerythritol core (PEGOA) [116], hyaluronic acid [117], PVA [118], or hydroxyapatite [119], are incorporated, they can enhance printability and/or improve shape fidelity post-bioprinting.

Furthermore, various bioactive materials such as fibrin (or fibrinogen and thrombin) and polylysine have been added to bioinks, for the induction or enhancement of their bioactivity. Fibrin, a polymer of fibrinogen that forms fibrous, viscoelastic, and porous hydrogels in the presence of thrombin, was shown to improve the bioadhesiveness and bioactivity of bioink [120]. Positively charged polylysine has also been used to enhance cell adhesion by increasing the electrostatic interactions with negatively charged cell membranes [121].

Similarly, the biochemical properties of non-adhesive hydrogels have been improved by their modification with adhesive peptide ligands. The arginine-glycine-aspartic acid (RGD) peptide is the most commonly used peptide ligand that plays a pivotal role in cell adhesion, spreading, and migration [122]. For example, PEG-diacrylate (PEGDA) hydrogels conjugated with RGD peptides enhanced the adhesion of cells as compared with those without RGD modifications [123]. It was further demonstrated that the inclusion of RGD peptides on implanted PEGDA hydrogels regulated cell adhesion, inflammation, fibrous encapsulation, and vascularization, *in vivo* [123]. RGD peptides have also been introduced to various other hydrogel-forming polymers, such as hyaluronic acid [123], alginate [124], chitosan [125], and PEG [126] hydrogels, to improve cell behaviors.

Several growth factors such as fibroblast growth factor (FGF), vascular endothelial growth factor (VEGF), and transforming growth factor-α (TGF-α) and TGF-β have been identified as the inducers of angiogenesis. For example, FGF-2 [127] and VEGF [128] are the key mediators of blood vessel formation that stimulate the proliferation, motility, and differentiation of ECs [129]. VEGF was physically entrapped within PEG hydrogels for release in response to proteases secreted by the cells, leading to enhanced vessel formation in both *in vitro* and *in vivo* studies [130]. Moreover, several growth factor-binding sites have been discovered within ECM proteins such as fibronectin [131], fibrinogen [132], tenascin C [133], and vitronectin [134]. VEGF bound to these ECM proteins has been shown to improve healing of diabetic wounds and bone defects [135]. While some of these strategies may have not been combined with bioinks for vascular bioprinting, their adaptation would seem to be natural.

More recently, several studies have shown the effect of altered substrate viscoelasticity on cell behaviors, including tuning the loss modulus of acrylamide hydrogels by altering the covalent crosslinking and/or concentration of the polymer [136,137], modulating stress relaxation in PEG hydrogels by altering covalent crosslinkers with different affinities [138], or using the covalent and/or physical crosslinking of alginate hydrogels [139]. These studies showed that an improved loss modulus and substrate creep enhanced the cell spreading and osteogenic differentiation of MSCs in two-dimensional (2D) culture [136,137], and that enhanced substrate stress relaxation improved the spreading and proliferation of cells in 2D [139] and allowed cells to adapt to physiologically relevant morphologies in 3D culture [138]. Similarly, it was demonstrated that cells behaved differently in elastic and viscoelastic hydrogels and that the relaxation behaviors of the biomaterial changed with the interaction of cells, altering cell behaviors including spreading, proliferation, and differentiation [140]. MSC differentiation was found to be dependent on the initial elastic modulus of the hydrogel in 3D, whereas it lost sensitivity to hydrogel stiffness in elastic hydrogels, indicating the significance of stress relaxation in cells with respect to mechanical cues in the ECM [141]. These insights may be helpful in vascular bioink designs for improving cell behaviors and vessel functions.

4. Current advances in the bioprinting of small-diameter vessels

Small vessels include the arteriolar and venules. The flow of blood through the capillaries is regulated by the arteriolar lumen. Venules are the smallest veins that receive blood from capillaries and play an important role in the exchange of oxygen and nutrients between the blood and tissue [4]. It is typically difficult to construct small-diameter blood vessels, including small vessels and microvessels, using a manual approach. However, with the advantages of bioprinting, more sophisticated and physiologically relevant structures of small-diameter blood vessels may be obtained [46,142].

4.1. Extrusion bioprinting

Extrusion bioprinting is a cost-effective and commonly used method of bioprinting, which dispenses the bioink from a printhead in a way that is synchronized with the printhead's spatial movement in a layer-by-layer manner [47,143,144]. Extrusion bioprinters dispense bioinks continuously through the nozzle pneumatically or mechanically, and are compatible with a wide range of bioinks with high viscosities [145]. Alginate has been extensively used in the extrusion bioprinting of vascular tissue constructs. For example, alginate can be physically crosslinked with simultaneously delivered calcium chloride ($CaCl_2$) solution in the core, to ensure the structural fidelity of the bioprinted hollow constructs [89,146]. Perfusable vasculature conduits were bioprinted with primary human umbilical vein SMCs (HUVSMCs) encapsulated in sodium alginate solution (3%, 4%, and 5% w/v in deionized water) using a coaxial nozzle, fabricated with an outer needle (ID = 540 μm) and a inner needle (ID = 250 μm) [147]. The average vascular conduit and lumen diameters bioprinted with sodium alginate solution (5% w/v) were (1449 ± 27) and (990 ± 16) μm, respectively. Similarly, 3D bioprinting of hollow calcium alginate fibers of uniform diameter with high mechanical strength and structural integrity was achieved with L929 mouse fibroblasts-encapsulated sodium alginate (2%–5% w/v) and $CaCl_2$ (2%–5% w/v) solutions, using the coaxial nozzle-assisted extrusion bioprinting method [148]. The coaxial assembly consisted of an outer needle with an ID of 1600 μm and three different inner needles of 510, 410, or 330 μm in ID. The size of the bioprinted hollow fibers varied depending on the size of the inner needles as well as the flow rate and concentration of sodium alginate and $CaCl_2$. The average inner and outer diameters of the bioprinted alginate hollow fibers were found to be 892 and 1192 μm, respectively, when sodium alginate solution (2% w/v at 1 $mL \cdot min^{-1}$ flow rate) and calcium chloride (4% w/v at 2 $mL \cdot min^{-1}$ flow rate) were used.

In another study, perusable vascular tissue constructs were fabricated using a multilayered coaxial nozzle with concentric needles, and a human umbilical vein ECs (HUVECs)- and human mesenchymal stem cells (hMSCs)-encapsulated bioink [110]. The bioink in this study was composed of sodium alginate (2% or 3% w/v), PEGTA (2% or 3% w/v), and GelMA (5% or 7% w/v) prepolymer solutions. PEGTA was added to enhance the mechanical

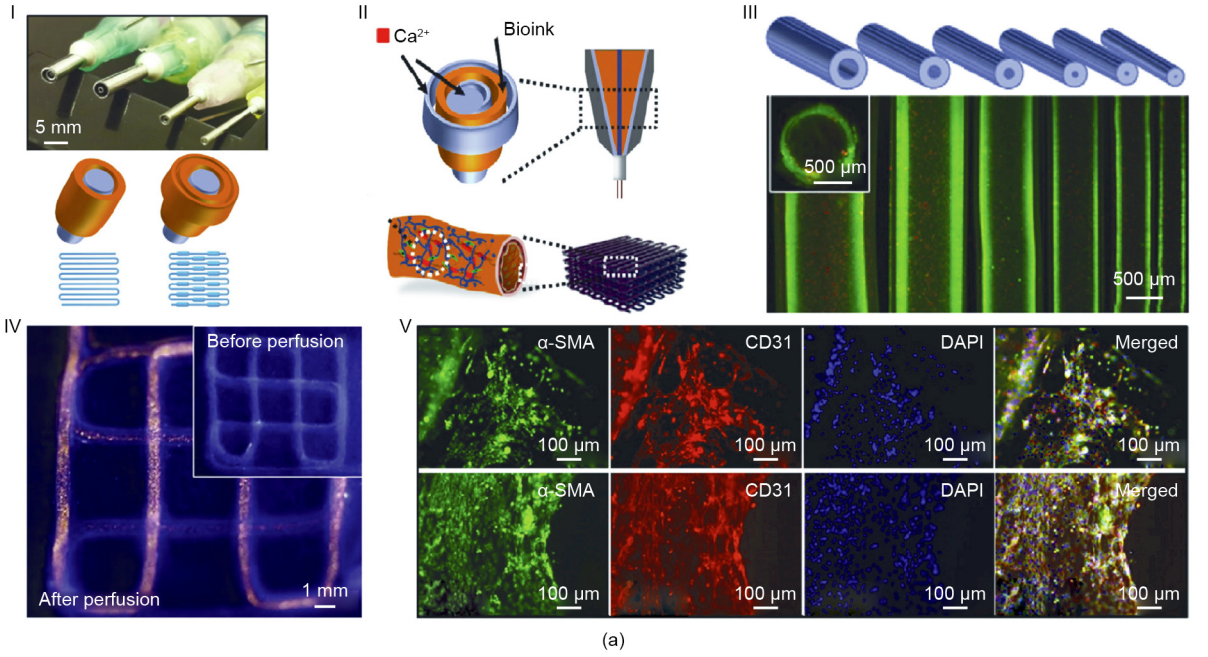

Fig. 3. (a) Coaxial bioprinting of small-diameter blood vessels. (I) Multilayered coaxial nozzles and schematics demonstrating the fabrication of various hollow tubes. (II) Schematics of the bioprinting process and fabrication of a vascular bed. (III) Schematics and fluorescence micrographs showing bioprinted tubes with varying diameters. (IV) Fluorescence photographs of bioprinted tubes before (inset) and after the injection of red fluorescent microbeads. (V) Confocal images of a vascular tubular structure showing the expression of smooth muscle α-actin (α-SMA) by MSCs and the expression of cluster of differentiation 31 (CD31) by HUVECs after 14 d (upper row) and 21 d (lower row) of culture. Nuclei are stained with 4′,6-diamidino-2-phenylindole (DAPI). (b) (I) Schematics showing a multichannel coaxial extrusion system for the bioprinting of a multilayered hollow tube. (II) Representative fluorescence micrographs of double-layered hollow tubes (upper row) and a cross-sectional view (lower row) of single- and double-layered hollow tubes. (III) Fluorescence micrographs of a bioprinted tube consisting of inner human urothelial cells labeled with green cell tracker and outer human bladder SMCs labeled with red cell tracker on Day 4. (IV) Confocal micrographs of immunostained vascular tubes exhibiting expression of CD31 (green) by HUVECs and α-SMA (red) by SMCs. (a) Reproduced from Ref. [110] with permission of Elsevier, © 2016; (b) reproduced from Ref. [116] with permission of Wiley, © 2018.

properties of the bioprinted vascular tissue constructs. Depending on the size of the inner (ID = 0.159–0.210 mm) and outer (ID = 0.153–0.838 mm) needles used, different-sized hollow tubes were bioprinted with the optimized blend bioink (3% w/v alginate, 2% w/v PEGTA, and 7% w/v GelMA). The average outer diameter (OD) of the bioprinted hollow tubes ranged approximately from 500 to 1500 μm, the ID ranged from 400 to 1000 μm, and the wall thickness ranged from 60 to 280 μm. The blended bioink was shown to support the spreading and proliferation of encapsulated HUVECs and MSCs in the bioprinted vascular constructs, thus forming physiologically relevant vascular tissue constructs (Fig. 3(a)) [110]. Recently, multilayered hollow vascular tissues were further fabricated using a multichannel coaxial extrusion system. The system consisted of a coaxial nozzle with three concentric needles (a needle in the core (ID = 0.210 mm), a needle in the middle layer (ID = 0.686 mm), and a needle in the outer layer (ID = 1.600 mm)); a bioink composed of GelMA (5% or 7% w/v), sodium alginate (2% or 3% w/v), and PEGOA (1% or 2% w/v); HUVECs to be delivered in the middle layer; and SMCs to be delivered in the outer layer [117]. When a blended bioink (7% w/v GelMA, 2% w/v alginate, and 2% w/v PEGOA) with optimal printability was used, the average diameter of the inner lumen was measured to be (663 ± 52) μm while that of the outer lumen was (977 ± 63) μm. The inner and outer wall thicknesses were found to be (62 ± 10) and (94 ± 10) μm, respectively (Fig. 3(b)) [116]. The bioprinted vascular tissues exhibited cellular heterogeneity of different layers and respective phenotypes, indicating the formation of blood vessel-like tissues.

In a more recent study, small-diameter blood vascular constructs comprising endothelial and muscular cell layers were fabricated with extrusion bioprinting, using a triple-layered coaxial nozzle (ID = 2.159/2.906/3.810 mm) with HUVECs and human aortic SMCs (HAoSMCs) encapsulated in vascular tissue-derived ECM (VdECM, 3% w/v)/alginate (2% w/v) hydrogel as the bioink [149]. The resultant tube of approximately 2 mm in ID consisted of a thin HUVEC layer (approximately 50 μm) surrounded by a thicker HAoSMC layer (800–1000 μm). The prematured vessel was then implanted into the abdominal aorta of rat for 21 d. The vascular graft showed smooth muscle layer remodeling and integration into the host tissue, along with good patency and an intact endothelium. Similarly, using a 3D-printed microfluidic coextrusion device, long permeable alginate tubes of (265 ± 11), (360 ± 11), or (448 ± 12) μm ODs were produced, which were subsequently seeded with HUVECs and vascular SMCs (vSMCs) co-encapsulated in Matrigel (35% v/v) [150]. The resulting vascular tubes possessed the correct configuration of lumen with an inner endothelial lining and an outer sheath of SMCs. These vascular tubes exhibited functional properties of vessels, including quiescence, perfusability, and contractility in response to vasoconstrictor agents. Another study presented the coaxial extrusion printing of small-diameter blood vessels, where human coronary artery SMCs (HCASMCs) were encapsulated in a catechol-functionalized GelMA (GelMA/C, 20 wt%) bioink [151]. The GelMA/C bioink with HCASMCs was extruded through an external larger needle (diameter: 840 μm), whereas the HUVECs in Pluronic F127 (30 wt%) and sodium periodate (23.4 $nmol \cdot L^{-1}$) were delivered through a smaller internal needle (diameter: 406 μm). Depending on the coaxial nozzles used, the IDs of the bioprinted tubes were found to be 500–1500 μm and the wall thickness ranged from 100 to 300 μm. The bioprinted vascular constructs were further implanted into nonobese diabetic-severe combined immunodeficiency (NOD-SCID) interleukin-2 (IL-2) receptor gamma null (NSG) mice, and suggested autonomous integration and functional vessel formation *in vivo*.

4.2. Inkjet bioprinting

Inkjet bioprinting is a fabrication method in which bioink droplets are deposited at predefined positions on a substrate. Formation of droplets may be induced by thermal or piezoelectric forces [48,152]. Alginate-based 3D tubular tissue constructs were fabricated with the sudden gelation of alginate beads in a $CaCl_2$ solution, thus forming microgel droplets as building blocks [153]. Specifically, sodium alginate solution (0.8% w/v) was ejected into a $CaCl_2$ solution (2% w/v) through an ink jet nozzle to form circular microgel beads of approximately 40 μm in diameter. Alginate tubes of 200 μm in diameter were fabricated by moving the inkjet printhead in a circular pattern, wherein droplets of the alginate gel were bioprinted in a bath of $CaCl_2$.

3D straight and zigzag cellular tubes of approximately 3 mm in diameter with overhung structures were successfully fabricated by layer-by-layer deposition with a 3D inkjet bioprinting system using NIH/3T3 fibroblasts encapsulated in sodium alginate (1% w/v) as the bioink [154]. The bioink droplets were ejected through a piezoelectric nozzle dispenser (ID = 120 μm) into a $CaCl_2$ (2% w/v) bath, forming a gelled cell-calcium alginate layer. The presented fabrication approach could potentially be applied for the bioprinting of blood vessels with complex geometries and structures. Similarly, vascular-like structures with bifurcations were generated by means of a liquid support-based inkjet bioprinting method. The bioink droplets, which were composed of sodium alginate solution (1% w/v) with or without NIH/3T3 fibroblasts, were ejected using a piezoelectric inkjet printhead (ID = 120 μm); $CaCl_2$ solution (2% w/v) was used as the crosslinking agent. The vascular constructs were bioprinted in either a horizontal manner (Figs. 4 (a-I), 4(a-II), 4(b-I), and 4(b-II)) or a vertical manner (Figs. 4(a-III), 4(a-IV), 4(b-III), and 4(b-IV)) into a bath of $CaCl_2$ solution (2% w/v). The mean diameter of the bifurcated vascular structure was 3 mm and the thickness of the wall was approximately 1 mm [35]. In another example, a bioink of thrombin (50 $U \cdot mL^{-1}$) and $CaCl_2$ (80 $mmol \cdot L^{-1}$) was mixed with human microvascular ECs (HMVECs) and deposited into a fibrinogen substrate (60 $mg \cdot mL^{-1}$; so-called "bio-paper") to form a fibrin channel of < 100 μm in diameter mimicking the microvascular structure. The bioprinted cells were aligned inside the fibrin channels and were ready for proliferation, and the channel structure of the bioprinted microvasculature were observed to remain stable for 21 d [155].

4.3. Laser-assisted and vat polymerization-based bioprinting

Laser-assisted bioprinting is a nozzle-free bioprinting approach that utilizes laser pulses to deposit the bioink from the donor slide onto the receiver [156]. A study demonstrated the potential of laser-assisted bioprinting for fabricating straight and Y-shaped tubular constructs using alginate (8% w/v) or alginate (2% w/v) containing mouse fibroblasts as bioinks. The average cellular Y-shaped constructs were 5 mm in diameter when optimized parameters were applied (laser fluence: 1445 $mJ \cdot cm^{-2}$, repetition rate: 10 Hz, substrate velocity: 80 $mm \cdot min^{-1}$, downward movement step size: 25 μm) [38]. Simple structures that mimicked the vascular networks in natural tissue were fabricated with HUVECs and HUVSMCs using laser-assisted bioprinting. Bioprinted droplets of approximately 50 μm in diameter were deposited 50–150 μm away from each other when a laser energy of 0.5–1.5 $\mu J \cdot pulse^{-1}$ was used [157].

Dynamic digital micro-mirror device (DMD)-based vat polymerization bioprinting is another fabrication method with high resolution [158]. This technique enables the fabrication of highly

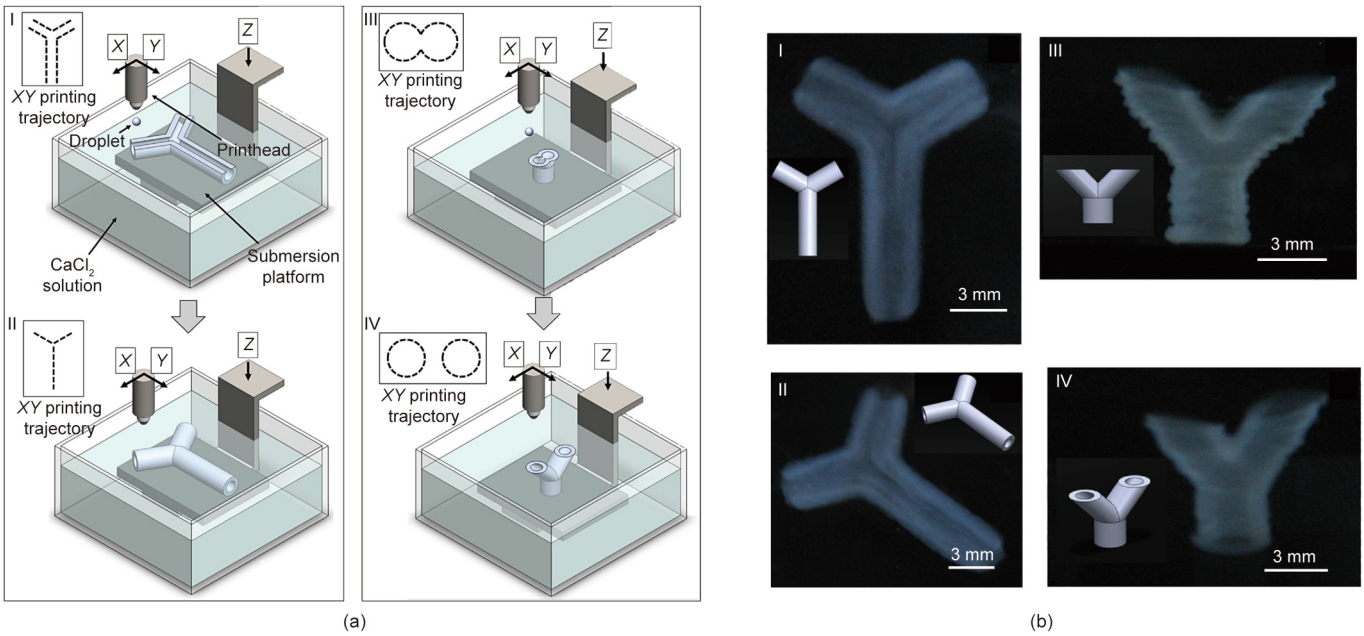

Fig. 4. Inkjet bioprinting of small-diameter blood vessels. (a) Schematics showing the inkjet bioprinting of (I, II) horizontal and (III, IV) vertical bifurcated tubular constructs in which sodium alginate droplets (1% w/v), with or without cells, were deposited on the platform and then crosslinked with $CaCl_2$ solution. (b) (I) Top view and (II) global view of bifurcated alginate tubes generated by horizontal printing; (III) front view and (IV) global view of bifurcated alginate tubes generated by vertical printing. Reproduced from Ref. [35] with permission of Wiley, © 2015.

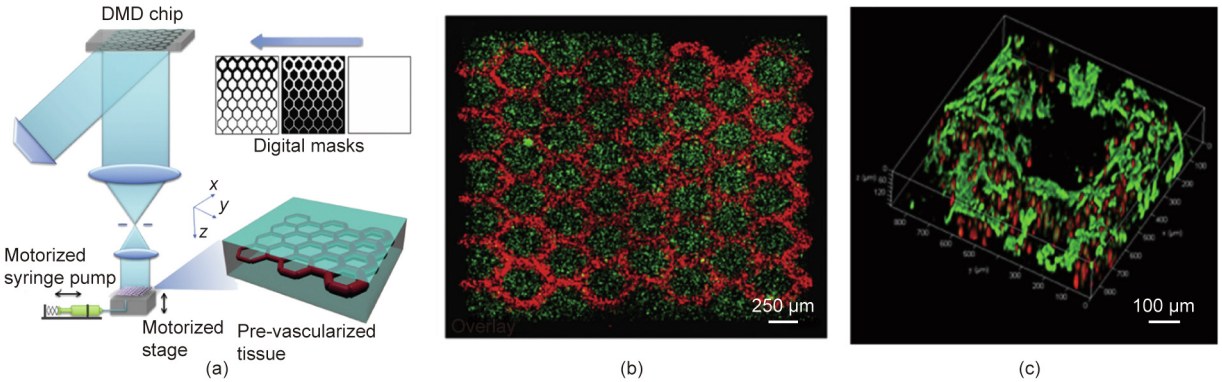

Fig. 5. Vat polymerization-based bioprinting of microvascularized tissues. (a) Schematics showing the fabrication of pre-vascularized tissue constructs; (b) fluorescence micrograph showing bioprinted tissue constructs consisting of HUVECs (red) in the channels and HepG2 cells (green) in the surrounding hydrogel matrix; (c) 3D confocal reconstruction micrograph showing ECs in microchannels, labeled with red cell tracker and stained for CD31 in green. Reproduced from Ref. [43] with permission of Elsevier, © 2013.

complex tissue constructs with micrometer resolution. Volumetric tissue constructs with embedded vasculature were fabricated using hydrogels encapsulating relevant cells [159]. For example, a 3D vascularized hepatic model was fabricated with a DMD-based stereolithographic bioprinting approach in which hepatic lobules were fabricated with human induced pluripotent stem cell (hiPSC)-derived hepatic cells encapsulated in GelMA (5% w/v), followed by the fabrication of vasculature using HUVECs and adipose-derived stem cells encapsulated in glycidal methacrylate-hyaluronic acid (1% w/v) and GelMA (2.5% w/v) [46]. These 3D-bioprinted liver construct, measuring 3 mm × 3 mm with a thickness of approximately 200 μm, consisted of a hexagonal array of hiPSC-derived hepatic cell lobules with surrounding layers of HUVECs and adipose-derived stem cells. This vascularized liver model provides a platform for pathophysiological and drug screening studies [46]. In another study, a pre-vascularized tissue construct were created following the same approach; three digital masks were employed to fabricate the patterned tissue constructs, with uniform (Fig. 5) [43] or gradient vascular channels forming the vasculature network [142]. The size of the vascular channels ranged from 50 to 250 μm. While the base layer of the vascularized tissue constructs consisted of hexagonal regions which was fabricated with HepG2 cells encapsulated in GelMA (5% w/v) using a digital mask with hexagonal patterns, the vascular channel region was fabricated with HUVECs and 10T1/2 murine embryo fibroblasts encapsulated in the hydrogel (2.5% w/v GelMA + 1% w/v glycidal methacrylate-hyaluronic acid) using the vascular channel mask. Finally, the vascular network was covered on the top with GelMA (5% w/v) using a slab mask, thus generating a vascularized tissue construct of 4 mm × 5 mm in size with a thickness of 600 μm. The HUVECs in

the bioprinted tissue construct spontaneously formed lumen-like structures *in vitro*. Furthermore, the bioprinted pre-vascularized and non-pre-vascularized (without cells) tissue constructs were implanted under the dorsal skin of severe combined immunodeficiency mice for 14 d and demonstrated endothelialization of the pre-vascularized tissue constructs [142].

4.4. Other bioprinting strategies

Besides the abovementioned bioprinting modalities for fabricating vasculature structures, sacrificial bioprinting is a classical indirect (bio)printing method. The sacrificial bioprinting of vascularized tissue constructs utilizes fugitive bioinks that are removed after the completion of the bioprinting, usually by physical extraction or changing the temperature, leaving behind the perfusable channels [62]. Cylindrical agarose fibers were bioprinted within cell-laden GelMA hydrogels by the extrusion bioprinting method, using agarose as the sacrificial template [88,160]. The agarose fibers were then removed, resulting in perfusable vessels within GelMA. The ID of these vessels ranged from 800 μm to 2 mm, while the wall thickness ranged from 50 to 100 μm. These perfusable vessels allowed increased mass transport in thick hydrogels and supported the formation of endothelial monolayers. A similar bioprinting approach was employed for the generation of hollow vasculature within GelMA hydrogels using Pluronic F127 [161]. HUVECs were perfused into the hollow channel to form EC monolayers.

As an alternative, a 3D vascularized network was created in which an open and interconnected sacrificial carbohydrate glass lattice was printed at 110 °C using a carbohydrate glass formulation (a mixture of 25 g of glucose, 53 g of sucrose, and 10 g of dextran in 50 mL of reverse-osmosis water), through a steel nozzle (ID = 1.2 or 0.84 mm) [162]. The printed carbohydrate glass lattice was then immersed in a poly(*d*-lactide-*co*-glycolide) solution after vitrification at 50 °C for 5 min, which prevented osmotic damage of the encapsulated cells due to carbohydrate dissolution. Various cell-laden hydrogels, including human embryonic kidney (HEK) 293 cell-laden PEG hydrogel (comprising PEG-diacrylate (5%, 10%, or 20% w/w) and 1 $mmol \cdot L^{-1}$ acrylate–PEG–arginine-glycine-aspartic acid-serine (RGDS) and Irgacure 2959 (0.05% w/v), 10T1/2 cell-laden fibrin gel (10 $mg \cdot mL^{-1}$, comprising fibrinogen and thrombin), 10T1/2 cell-laden alginate gel (2% w/v), primary rat hepatocyte- and stromal fibroblast-loaded agarose gels (2% w/v), and 10T1/2 cell-laden Matrigel, were used to encapsulate the 3D-printed glass lattices. Following ECM crosslinking, the sacrificial carbohydrate glass was removed by immersing the whole structure in medium, leaving behind open channels within the ECM hydrogel. These vascular channels were lined with HUVECs, followed by perfusion with blood under high-pressure pulsatile flows. It was revealed that these vascular channels were able to support the metabolic function of primary rat hepatocytes in the 3D bioprinted tissue constructs. Following the same approach, sacrificial carbohydrate glass filaments were printed using 100 g of isomalt and 10 g of dextran in 60 mL of reverse-osmosis water, through a steel nozzle (ID = 0.84 mm), which was encapsulated within a fibrin gel (10 $mg \cdot mL^{-1}$) [163]. The sacrificial carbohydrate filaments were removed by washing with phosphate-buffered saline (PBS), followed by the injection of HUVECS into the hollow channels. These 3D-printed vascular patches were implanted in a mouse model of hind limb ischemia, and demonstrated enhanced angiogenesis and the integration of engineered vessels with the host vasculature, resulting in perfusion of distal ischemic tissues. Similarly, when applied in a myocardial infarction mouse model, these bioprinted vascular patches were demonstrated to partially rescue cardiac function, with an ejection fraction and a cardiac output similar to those in the healthy controls.

In another study, two fluidic vascular channels were created within a 3D collagen I matrix (3 $mg \cdot mL^{-1}$) using gelatin (10% w/v) as a sacrificial material; the collagen precursor was first bioprinted on a flow chamber, followed by the bioprinting of two gelatin fibers [164]. After the deposition of HUVECs and normal human lung fibroblasts encapsulated in a fibrin gel in between two gelatin fibers, several layers of collagen were bioprinted on top to cover the entire structure. The sacrificial gelatin was then removed and HUVECs were injected into the channels, which were later allowed to flow with medium. The study demonstrated the formation of a microvasculature network by embedding HUVECs and fibroblasts within the fibrin gel in between the two vascular channels.

Recently, a drop-on-demand bioprinting method for producing blood vessel constructs was demonstrated using a bioprinter with three printheads [10,11]. Gelatin (5% w/v) or HUVEC-loaded gelatin (3% w/v) was bioprinted as a sacrificial core using a printhead of 150 μm in diameter. Two other printheads of 0.3 mm in diameter were used to fabricate the muscle layer; one printhead dispensed droplets of crosslinker solution, containing thrombin, transglutaminase, and $CaCl_2$, while the other printhead dispensed the droplets of fibrinogen (2.5% w/v)-human umbilical artery SMC suspension. Finally, after the completion of the bioprinting process, the outer layer of the blood vessel was formed by casting a fibrinogen (1.25% w/v)–collagen (0.18% v/v) blend encapsulating normal human dermal fibroblasts around the muscle layer. Thus, the resulting perfusable vascular channel, with a diameter of 1 mm and a wall thickness of up to 425 μm, consisted of an endothelium, an SMC layer, and a surrounding matrix of fibroblasts.

Table 3
Representative parameters and properties of bioprinted small-diameter blood vessels.

Bioink	Bioprinting modality	Cell type	Vessel diameter	Reference
Agarose	Inkjet	HUVSMCs, HSFs	OD = 0.9–2.5 mm	[153]
VdECM/alginate	Extrusion	HUVECs	ID = 892 μm OD = 1192 μm	[148]
GelMA/alginate/PEGTA	Extrusion	HUVECs, hMSCs	ID = 400–1000 μm OD = 500–1500 μm	[110]
GelMA/alginate/PEGOA	Extrusion	HUVECs, SMCs	ID ≈ 663 μm OD ≈ 977 μm	[116]
VdECM/alginate	Extrusion	HUVECs, HAoSMCs	ID = 2 mm	[149]
Alginate	Extrusion	HUVECs, vSMCs	OD = 300 μm	[150]
GelMA/C	Extrusion	HUVECs, HCASMCs	ID = 500–1500 μm	[151]

HSFs: human skin fibroblasts.

5. Future directions

Advances in bioprinting technology have led to the bioengineering of perfusable blood vessel structures and vascularized tissue constructs with different shapes, sizes, and functions (Table 3) [110,116,148–151,153]. However, most bioprinted vascular tissues still lack the key structural components, mechanical properties, and physiological features of native blood vessels. Each bioprinting modality has its own advantages and disadvantages. An ideal modality should have maximized capacities such as resolution and bioprinting speed, and should be applicable to a wide range of bioinks with optimal vascularization potential in a vessel type-specific manner. Most previous studies have used HUVECs as a model cell type. Nevertheless, in order to achieve clinically relevant vascular tissue formation, bioprinted vascular constructs should be able to undergo remodeling and functional transition with relevant cell sources. Therefore, more efforts are required to explore improved bioprinting processes, as well as the development of advanced bioinks for fabricating functional small-diameter vascular grafts and vascularized tissue grafts with appropriate mechanical behaviors and favorable biological performances. Some of these biological performances may be facilitated further by incorporating dynamic culture conditions, such as perfusion bioreactors, to enhance maturation. Finally, a continued understanding of vascular biology, including the interactions between different layers of blood vessels such as ECs, SMCs, surrounding supporting cells, and the ECM, will provide better insights toward improved engineering designs.

Acknowledgements

This work was supported by funding from the US National Institutes of Health (R00CA201603, R21EB025270, R21EB026175, and R01EB028143) and the Brigham Research Institute.

Compliance with ethics guidelines

Xia Cao, Sushila Maharjan, Ramla Ashfaq, Jane Shin, and Yu Shrike Zhang declare that they have no conflict of interest or financial conflicts to disclose.

References

[1] Brewster L, Brey EM, Greisler HP. Blood vessels. In: Lanza R, Langer R, Vacanti J, editors. Principles of tissue engineering. Boston: Academic Press; 2014. p. 793–812.
[2] Chang WG, Niklason LE. A short discourse on vascular tissue engineering. NPJ Regen Med 2017;2:7.
[3] Ardalani H, Assadi AH, Murphy WL. Structure, function, and development of blood vessels: lessons for tissue engineering. In: Cai W, editor. Engineering in translational medicine. London: Springer; 2014. p. 155–82.
[4] Tucker WD, Arora Y. Anatomy, blood vessels [Internet]. Treasure Island: StatPearls Publishing; c2020 [updated 2020 Aug 10; cited 2020 Aug 21]. Available from: https://www.statpearls.com/kb/viewarticle/32153/.
[5] Miri AK, Khalilpour A, Cecen B, Maharjan S, Shin SR, Khademhosseini AJB. Multiscale bioprinting of vascularized models. Biomaterials 2019;198:204–16.
[6] Hurst JW, Logue RB, Schlant RC, Wenger NK, editors. The heart: arteries and veins. New York: McGraw-Hill; 1978.
[7] SEER training modules—classification & structure of blood vessels [Internet]. National Cancer Institute at the US National Institutes of Health; [cited 2020 Aug 21]. Available from: https://training.seer.cancer.gov/anatomy/cardiovascular/blood/classification.html.
[8] Hammes M. Hemodynamic and biologic determinates of arteriovenous fistula outcomes in renal failure patients. BioMed Res Int 2015;2015:171674.
[9] Bergers G, Song S. The role of pericytes in blood-vessel formation and maintenance. Neuro Oncol 2005;7(4):452–64.
[10] Schöneberg J, De Lorenzi F, Theek B, Blaeser A, Rommel D, Kuehne AJ, et al. Engineering biofunctional *in vitro* vessel models using a multilayer bioprinting technique. Sci Rep 2018;8:10430.
[11] Burton AC. Relation of structure to function of the tissues of the wall of blood vessels. Physiol Rev 1954;34(4):619–42.
[12] Nemeno-Guanzon JG, Lee S, Berg JR, Jo YH, Yeo JE, Nam BM, et al. Trends in tissue engineering for blood vessels. BioMed Res Int 2012;2012:956345.
[13] Post A, Wang E, Cosgriff-Hernandez E. A review of integrin-mediated endothelial cell phenotype in the design of cardiovascular devices. Ann Biomed Eng 2019;47:366–80.
[14] Li M, Qian M, Kyler K, Xu J. Endothelial-vascular smooth muscle cells interactions in atherosclerosis. Front Cardiovasc Med 2018;5:151.
[15] Aird WC. Endothelial cell heterogeneity. Cold Spring Harb Perspect Med 2012;2(1):a006429.
[16] Hwa C, Sebastian A, Aird WC. Endothelial biomedicine: its status as an interdisciplinary field, its progress as a basic science, and its translational bench-to-bedside gap. Endothelium 2005;12(3):139–51.
[17] Muller WA. Getting leukocytes to the site of inflammation. Vet Pathol 2013;50(1):7–22.
[18] Steucke KE, Tracy PV, Hald ES, Hall JL, Alford PW. Vascular smooth muscle cell functional contractility depends on extracellular mechanical properties. J Biomech 2015;48(12):3044–51.
[19] Mathers CD, Loncar DJP. Projections of global mortality and burden of disease from 2002 to 2030. PLoS Med 2006;3(11):e442.
[20] Pashneh-Tala S, MacNeil S, Claeyssens F. The tissue-engineered vascular graft—past, present, and future. Tissue Eng Part B Rev 2015;22(1):68–100.
[21] Taylor LM, Edwards JM, Brant B, Phinney ES, Porter JM. Autogenous reversed vein bypass for lower extremity ischemia in patients with absent or inadequate greater saphenous vein. Am J Surg 1987;153(5):505–10.
[22] Harskamp RE, Lopes RD, Baisden CE, de Winter RJ, Alexander JH. Saphenous vein graft failure after coronary artery bypass surgery: pathophysiology, management, and future directions. Ann Surg 2013;257(5):824–33.
[23] Ma Z, Kotaki M, Yong T, He W, Ramakrishna S. Surface engineering of electrospun polyethylene terephthalate (PET) nanofibers towards development of a new material for blood vessel engineering. Biomaterials 2005;26(15):2527–36.
[24] Lord MS, Yu W, Cheng B, Simmons A, Poole-Warren L, Whitelock JM. The modulation of platelet and endothelial cell adhesion to vascular graft materials by perlecan. Biomaterials 2009;30(28):4898–906.
[25] Catto V, Farè S, Freddi G, Tanzi MC. Vascular tissue engineering: recent advances in small diameter blood vessel regeneration. Vasc Med 2014;2014:923030.
[26] Bordenave L, Menu P, Baquey C. Developments towards tissue-engineered, small-diameter arterial substitutes. Expert Rev Med Devices 2008;5(3):337–47.
[27] Dean EW, Udelsman B, Breuer CK. Current advances in the translation of vascular tissue engineering to the treatment of pediatric congenital heart disease. Yale J Biol Med 2012;85(2):229–38.
[28] Tara S, Rocco KA, Hibino N, Sugiura T, Kurobe H, Breuer CK, et al. Vessel bioengineering. Circ J 2013;78(1):12–9.
[29] Han X, Bibb R, Harris RJB. Engineering design of artificial vascular junctions for 3D printing. Biofabrication 2016;8(2):025018.
[30] Hoch E, Tovar GE, Borchers K. Bioprinting of artificial blood vessels: current approaches towards a demanding goal. Eur J Cardiothorac Surg 2014;46(5):767–78.
[31] Murphy SV, Atala A. 3D bioprinting of tissues and organs. Nat Biotechnol 2014;32(8):773–85.
[32] Li J, Chen M, Fan X, Zhou H. Recent advances in bioprinting techniques: approaches, applications and future prospects. J Transl Med 2016;14:271.
[33] Dimitrievska S, Niklason LE. Historical perspective and future direction of blood vessel developments. Cold Spring Harb Perspect Med 2017;8(2):a025742.
[34] Datta P, Ayan B, Ozbolat IT. Bioprinting for vascular and vascularized tissue biofabrication. Acta Biomater 2017;51:1–20.
[35] Christensen K, Xu C, Chai W, Zhang Z, Fu J, Huang Y. Freeform inkjet printing of cellular structures with bifurcations. Biotechnol Bioeng 2015;112(5):1047–55.
[36] Yu Y, Zhang Y, Martin JA, Ozbolat IT. Evaluation of cell viability and functionality in vessel-like bioprintable cell-laden tubular channels. J Biomech Eng 2013;135(9):091011.
[37] Zhang Y, Yu Y, Ozbolat IT. Direct bioprinting of vessel-like tubular microfluidic channels. J Nanotechnol Eng Med 2013;4(2):020902.
[38] Xiong R, Zhang Z, Chai W, Huang Y, Chrisey DB. Freeform drop-on-demand laser printing of 3D alginate and cellular constructs. Biofabrication 2015;7(4):045011.
[39] Heinrich MA, Liu W, Jimenez A, Yang J, Akpek A, Liu X, et al. 3D bioprinting: from benches to translational applications. Small 2019;15(23):1805510.
[40] Maina RM, Barahona MJ, Finotti M, Lysyy T, Geibel P, D'Amico F, et al. Generating vascular conduits: from tissue engineering to three-dimensional bioprinting. Innov Surg Sci 2018;3(3):203–13.
[41] Bishop ES, Mostafa S, Pakvasa M, Luu HH, Lee MJ, Wolf JM, et al. 3-D bioprinting technologies in tissue engineering and regenerative medicine: current and future trends. Genes Dis 2017;4(4):185–95.
[42] Seol YJ, Kang HW, Lee SJ, Atala A, Yoo JJ. Bioprinting technology and its applications. Eur J Cardiothorac Surg 2014;46(3):342–8.

[43] Guillotin B, Ali M, Ducom A, Catros S, Keriquel V, Souquet A, et al. Laser-assisted bioprinting for tissue engineering. In: Forgacs G, Sun W, editors. Biofabrication. Amsterdam: Elsevier Inc.; 2013. p. 95–118.
[44] Malda J, Visser J, Melchels FP, Jungst T, Hennink WE, Dhert WJA, et al. 25th anniversary article: engineering hydrogels for biofabrication. Adv Mater 2013;25(36):5011–28.
[45] Wang Z, Abdulla R, Parker B, Samanipour R, Ghosh S, Kim K. A simple and high-resolution stereolithography-based 3D bioprinting system using visible light crosslinkable bioinks. Biofabrication 2015;7(4):045009.
[46] Ma X, Qu X, Zhu W, Li YS, Yuan S, Zhang H, et al. Deterministically patterned biomimetic human iPSC-derived hepatic model via rapid 3D bioprinting. Proc Natl Acad Sci USA 2016;113:2206–11.
[47] Kirchmajer DM, Gorkin R, Panhuis MIH. An overview of the suitability of hydrogel-forming polymers for extrusion-based 3D-printing. J Mater Chem B 2015;3(20):4105–17.
[48] Boland T, Xu T, Damon B, Cui X. Application of inkjet printing to tissue engineering. Biotechnol J 2006;1(9):910–7.
[49] Xu T, Jin J, Gregory C, Hickman JJ, Boland T. Inkjet printing of viable mammalian cells. Biomaterials 2005;26(1):93–9.
[50] Panwar A, Tan LP. Current status of bioinks for micro-extrusion-based 3D bioprinting. Molecules 2016;21(6):685.
[51] Urrios A, Parra-Cabrera C, Bhattacharjee N, Gonzalez-Suarez AM, Rigat-Brugarolas LG, Nallapatti U, et al. 3D-printing of transparent bio-microfluidic devices in PEG-DA. Lab Chip 2016;16(12):2287–94.
[52] Raman R, Bashir R. Stereolithographic 3D bioprinting for biomedical applications. In: Essentials of 3D biofabrication and translation. Amsterdam: Elsevier; 2015. p. 89–121.
[53] LaValley DJ, Reinhart-King C. Matrix stiffening in the formation of blood vessels. Adv Regener Bio 2014;1(1):25247.
[54] Davis GE, Senger DR. Endothelial extracellular matrix: biosynthesis, remodeling, and functions during vascular morphogenesis and neovessel stabilization. Circ Res 2005;97(11):1093–107.
[55] Kniazeva E, Putnam AJ. Endothelial cell traction and ECM density influence both capillary morphogenesis and maintenance in 3-D. Am J Physiol Cell Physiol 2009;297(1):C179–87.
[56] Wagenseil JE, Mecham RP. Vascular extracellular matrix and arterial mechanics. Physiol Rev 2009;89(3):957–89.
[57] Yurchenco PD. Basement membranes: cell scaffoldings and signaling platforms. Cold Spring Harb Perspect Biol 2011;3(2):a004911.
[58] Lacolley P, Regnault V, Segers P, Laurent S. Vascular smooth muscle cells and arterial stiffening: relevance in development, aging, and disease. Physiol Rev 2017;97(4):1555–617.
[59] Bou-Gharios G, Ponticos M, Rajkumar V, Abraham D. Extra-cellular matrix in vascular networks. Cell Prolif 2004;37(3):207–20.
[60] Hallmann R, Horn N, Selg M, Wendler O, Pausch F, Sorokin LM. Expression and function of laminins in the embryonic and mature vasculature. Physiol Rev 2005;85(3):979–1000.
[61] Neve A, Cantatore FP, Maruotti N, Corrado A, Ribatti D. Extracellular matrix modulates angiogenesis in physiological and pathological conditions. BioMed Res Int 2014;2014:756078.
[62] Richards D, Jia J, Yost M, Markwald R, Mei Y. 3D bioprinting for vascularized tissue fabrication. Ann Biomed Eng 2017;45(1):132–47.
[63] Chimene D, Lennox KK, Kaunas RR, Gaharwar AK. Advanced bioinks for 3D printing: a materials science perspective. Ann Biomed Eng 2016;44(6):2090–102.
[64] Mandrycky C, Wang Z, Kim K, Kim DH. 3D bioprinting for engineering complex tissues. Biotechnol Adv 2016;34(4):422–34.
[65] Rutz AL, Hyland KE, Jakus AE, Burghardt WR, Shah RN. A multimaterial bioink method for 3D printing tunable, cell-compatible hydrogels. Adv Mater 2015;27(9):1607–14.
[66] Xu Y, Hu Y, Liu C, Yao H, Liu B, Mi S. A novel strategy for creating tissue-engineered biomimetic blood vessels using 3D bioprinting technology. Materials 2018;11(9):1581.
[67] Knight E, Przyborski S. Advances in 3D cell culture technologies enabling tissue-like structures to be created *in vitro*. J Anat 2015;227(6):746–56.
[68] Skardal A, Zhang J, McCoard L, Xu X, Oottamasathien S, Prestwich GD. Photocrosslinkable hyaluronan-gelatin hydrogels for two-step bioprinting. Tissue Eng Part A 2010;16(8):2675–85.
[69] Liu J, Hwang HH, Wang P, Whang G, Chen S. Direct 3D-printing of cell-laden constructs in microfluidic architectures. Lab Chip 2016;16(8):1430–8.
[70] Trappmann B, Baker BM, Polacheck WJ, Choi CK, Burdick JA, Chen CS. Matrix degradability controls multicellularity of 3D cell migration. Nat Commun 2017;8:371.
[71] Sakai S, Hirose K, Taguchi K, Ogushi Y, Kawakami K. An injectable, *in situ* enzymatically gellable, gelatin derivative for drug delivery and tissue engineering. Biomaterials 2009;30(20):3371–7.
[72] Seliktar D, Black RA, Vito RP, Nerem RM. Dynamic mechanical conditioning of collagen-gel blood vessel constructs induces remodeling *in vitro*. Ann Biomed Eng 2000;28(4):351–62.
[73] Boccafoschi F, Habermehl J, Vesentini S, Mantovani D. Biological performances of collagen-based scaffolds for vascular tissue engineering. Biomaterials 2005;26(35):7410–7.
[74] Boccafoschi F, Rajan N, Habermehl J, Mantovani D. Preparation and characterization of a scaffold for vascular tissue engineering by direct-assembling of collagen and cells in a cylindrical geometry. Macromol Biosci 2007;7(5):719–26.
[75] Amadori L, Rajan N, Vesentini S, Mantovani D. Atomic force and confocal microscopic studies of collagen-cell-based scaffolds for vascular tissue engineering. Adv Mater Res 2007;15–7:83–8.
[76] Schutte SC, Chen Z, Brockbank KGM, Nerem RM. Cyclic strain improves strength and function of a collagen-based tissue-engineered vascular media. Tissue Eng Part A 2010;16(10):3149–57.
[77] Kolesky DB, Homan KA, Skylar-Scott MA, Lewis JA. Three-dimensional bioprinting of thick vascularized tissues. Proc Natl Acad Sci USA 2016;113(12):3179–84.
[78] Leach JB, Wolinsky JB, Stone PJ, Wong JY. Crosslinked α-elastin biomaterials: towards a processable elastin mimetic scaffold. Acta Biomater 2005;1(2):155–64.
[79] McKenna KA, Hinds MT, Sarao RC, Wu PC, Maslen CL, Glanville RW, et al. Mechanical property characterization of electrospun recombinant human tropoelastin for vascular graft biomaterials. Acta Biomater 2012;8(1):225–33.
[80] Çelebi B, Cloutier M, Balloni R, Mantovani D, Bandiera A. Human elastin-based recombinant biopolymers improve mesenchymal stem cell differentiation. Macromol Biosci 2012;12(11):1546–54.
[81] Patel A, Fine B, Sandig M, Mequanint K. Elastin biosynthesis: the missing link in tissue-engineered blood vessels. Cardiovasc Res 2006;71(1):40–9.
[82] Swartz DD, Russell JA, Andreadis ST. Engineering of fibrin-based functional and implantable small-diameter blood vessels. Am J Physiol Heart Circ Physiol 2005;288(3):H1451–60.
[83] Ye Q, Zünd G, Benedikt P, Jockenhoevel S, Hoerstrup SP, Sakyama S, et al. Fibrin gel as a three dimensional matrix in cardiovascular tissue engineering. Eur J Cardiothorac Surg 2000;17(5):587–91.
[84] Yao L, Swartz DD, Gugino SF, Russell JA, Andreadis ST. Fibrin-based tissue-engineered blood vessels: differential effects of biomaterial and culture parameters on mechanical strength and vascular reactivity. Tissue Eng 2005;11(7–8):991–1003.
[85] Swartz DD, Russell JA, Andreadis ST, Physiology C. Engineering of fibrin-based functional and implantable small-diameter blood vessels. AJP Heart Circ Physiol 2005;288(3):H1451–60.
[86] Zavan B, Vindigni V, Lepidi S, Iacopetti I, Avruscio G, Abatangelo G, et al. Neoarteries grown *in vivo* using a tissue-engineered hyaluronan-based scaffold. FASEB J 2008;22(8):2853–61.
[87] Li S, Nih LR, Bachman H, Fei P, Li Y, Nam E, et al. Hydrogels with precisely controlled integrin activation dictate vascular patterning and permeability. Nat Mater 2017;16(9):953–61.
[88] Bertassoni LE, Cecconi M, Manoharan V, Nikkhah M, Hjortnaes J, Cristino AL, et al. Hydrogel bioprinted microchannel networks for vascularization of tissue engineering constructs. Lab Chip 2014;14(13):2202–11.
[89] Lee KY, Mooney DJ. Alginate: properties and biomedical applications. Prog Polym Sci 2012;37(1):106–26.
[90] Jia J, Richards DJ, Pollard S, Tan Y, Rodriguez J, Visconti RP, et al. Engineering alginate as bioink for bioprinting. Acta Biomater 2014;10(10):4323–31.
[91] Vernon RB, Sage EH. Between molecules and morphology: extracellular matrix and creation of vascular form. Am J Pathol 1995;147(4):873–83.
[92] Vernon RB, Angello JC, Iruela-Arispe ML, Lane TF, Sage EH. Reorganization of basement membrane matrices by cellular traction promotes the formation of cellular networks *in vitro*. Lab Invest 1992;66(5):536–47.
[93] Benton G, Arnaoutova I, George J, Kleinman HK, Koblinski J. Matrigel: from discovery and ECM mimicry to assays and models for cancer research. Adv Drug Deliv Rev 2014;79–80:3–18.
[94] Thottappillil N, Nair PD. Scaffolds in vascular regeneration: current status. Vasc Health Risk Manag 2015;11:79–91.
[95] Seifu DG, Purnama A, Mequanint K, Mantovani D. Small-diameter vascular tissue engineering. Nat Rev Cardiol 2013;10(7):410–21.
[96] Kim P, Yuan A, Nam KH, Jiao A, Kim DH. Fabrication of poly (ethylene glycol): gelatin methacrylate composite nanostructures with tunable stiffness and degradation for vascular tissue engineering. Biofabrication 2014;6(2):024112.
[97] Zhu J. Bioactive modification of poly(ethylene glycol) hydrogels for tissue engineering. Biomaterials 2010;31(17):4639–56.
[98] Madden LR, Mortisen DJ, Sussman EM, Dupras SK, Fugate JA, Cuy JL, et al. Proangiogenic scaffolds as functional templates for cardiac tissue engineering. Proc Natl Acad Sci USA 2010;107(34):15211–6.
[99] Conconi MT, Borgio L, Di Liddo R, Sartore L, Dalzoppo D, Amistà P, et al. Evaluation of vascular grafts based on polyvinyl alcohol cryogels. Mol Med Rep 2014;10(3):1329–34.
[100] Vrana NE, Liu Y, McGuinness GB, Cahill PA. Characterization of poly(vinyl alcohol)/chitosan hydrogels as vascular tissue engineering scaffolds. Macromol Symp 2008;269(1):106–10.
[101] Zhang YS, Khademhosseini AJS. Advances in engineering hydrogels. Science 2017;356(6337):eaaf3627.
[102] Schuurman W, Levett PA, Pot MW, van Weeren PR, Dhert WJ, Hutmacher DW, et al. Gelatin-methacrylamide hydrogels as potential biomaterials for fabrication of tissue-engineered cartilage constructs. Macromol Biosci 2013;13(5):551–61.
[103] Hu W, Wang Z, Xiao Y, Zhang S, Wang J. Advances in crosslinking strategies of biomedical hydrogels. Biomater Sci 2019;7(3):843–55.
[104] Zhou M, Lee BH, Tan LP. A dual crosslinking strategy to tailor rheological properties of gelatin methacryloyl. Int J Bioprint 2017;3(2):1–8.

[105] Shin H, Olsen BD, Khademhosseini A. The mechanical properties and cytotoxicity of cell-laden double-network hydrogels based on photocrosslinkable gelatin and gellan gum biomacromolecules. Biomaterials 2012;33(11):3143–52.
[106] Gaudet ID, Shreiber DI. Characterization of methacrylated type-I collagen as a dynamic, photoactive hydrogel. Biointerphases 2012;7(1–4):25.
[107] Pupkaite J, Ahumada M, Mclaughlin S, Temkit M, Alaziz S, Seymour R, et al. Collagen-based photoactive agent for tissue bonding. ACS Appl Mater Interfaces 2017;9(11):9265–70.
[108] Ondeck MG, Engler AJ. Mechanical characterization of a dynamic and tunable methacrylated hyaluronic acid hydrogel. J Biomech Eng 2016;138(2):021003.
[109] Poldervaart MT, Goversen B, de Ruijter M, Abbadessa A, Melchels FP, Öner FC, et al. 3D bioprinting of methacrylated hyaluronic acid (MeHA) hydrogel with intrinsic osteogenicity. PLoS ONE 2017;12(6):e0177628.
[110] Jia W, Gungor-Ozkerim PS, Zhang YS, Yue K, Zhu K, Liu W, et al. Direct 3D bioprinting of perfusable vascular constructs using a blend bioink. Biomaterials 2016;106:58–68.
[111] Pan T, Song W, Cao X, Wang Y. 3D bioplotting of gelatin/alginate scaffolds for tissue engineering: influence of crosslinking degree and pore architecture on physicochemical properties. J Mater Sci Technol 2016;32(9):889–900.
[112] Rich H, Odlyha M, Cheema U, Mudera V, Bozec L. Effects of photochemical riboflavin-mediated crosslinks on the physical properties of collagen constructs and fibrils. J Mater Sci Mater Med 2014;25(1):11–21.
[113] Jang J, Kim TG, Kim BS, Kim SW, Kwon SM, Cho DW. Tailoring mechanical properties of decellularized extracellular matrix bioink by vitamin B2-induced photo-crosslinking. Acta Biomater 2016;33:88–95.
[114] Bae HJ, Darby DO, Kimmel RM, Park HJ, Whiteside WS. Effects of transglutaminase-induced cross-linking on properties of fish gelatin–nanoclay composite film. Food Chem 2009;114(1):180–9.
[115] Schütz K, Placht AM, Paul B, Brüggemeier S, Gelinsky M, Lode A. Three-dimensional plotting of a cell-laden alginate/methylcellulose blend: towards biofabrication of tissue engineering constructs with clinically relevant dimensions. J Tissue Eng Regener Med 2017;11(5):1574–87.
[116] Pi Q, Maharjan S, Yan X, Liu X, Singh B, van Genderen AM, et al. Digitally tunable microfluidic bioprinting of multilayered cannular tissues. Adv Mater 2018;30(43):1706913.
[117] Rajaram A, Schreyer D, Chen D. Bioplotting alginate/hyaluronic acid hydrogel scaffolds with structural integrity and preserved schwann cell viability. 3D Print Addit Manuf 2014;1(4):194–203.
[118] Zhang J, Zhao S, Zhu Y, Huang Y, Zhu M, Tao C, et al. Three-dimensional printing of strontium-containing mesoporous bioactive glass scaffolds for bone regeneration. Acta Biomater 2014;10(5):2269–81.
[119] Wüst S, Godla ME, Müller R, Hofmann S. Tunable hydrogel composite with two-step processing in combination with innovative hardware upgrade for cell-based three-dimensional bioprinting. Acta Biomater 2014;10(2):630–40.
[120] Keating M, Lim M, Hu Q, Botvinick E. Selective stiffening of fibrin hydrogels with micron resolution via photocrosslinking. Acta Biomater 2019;87:88–96.
[121] Cui H, Zhu W, Holmes B, Zhang LG. Biologically inspired smart release system based on 3D bioprinted perfused scaffold for vascularized tissue regeneration. Adv Sci 2016;3(8):1600058.
[122] Huettner N, Dargaville TR, Forget A. Discovering cell-adhesion peptides in tissue engineering: beyond RGD. Trends Biotechnol 2018;36(4):372–83.
[123] Lee TT, García JR, Paez JI, Singh A, Phelps EA, Weis S, et al. Light-triggered *in vivo* activation of adhesive peptides regulates cell adhesion, inflammation and vascularization of biomaterials. Nat Mater 2015;14(3):352–60.
[124] Sun J, Wei D, Yang K, Yang Y, Liu X, Fan H, et al. The development of cell-initiated degradable hydrogel based on methacrylated alginate applicable to multiple microfabrication technologies. J Mater Chem B 2017;5(40):8060–9.
[125] Kim S, Cui ZK, Fan J, Fartash A, Aghaloo TL, Lee M. Photocrosslinkable chitosan hydrogels functionalized with the RGD peptide and phosphoserine to enhance osteogenesis. J Mater Chem B Mater Biol Med 2016;4(31):5289–98.
[126] Long J, Kim H, Kim D, Lee JB, Kim D. A biomaterial approach to cell reprogramming and differentiation. J Mater Chem B Mater Biol Med 2017;5(13):2375–89.
[127] Presta M, Dell'Era P, Mitola S, Moroni E, Ronca R, Rusnati M. Fibroblast growth factor/fibroblast growth factor receptor system in angiogenesis. Cytokine Growth Factor Rev 2005;16(2):159–78.
[128] Hoeben A, Landuyt B, Highley MS, Wildiers H, Van Oosterom AT, De Bruijn E. Vascular endothelial growth factor and angiogenesis. Pharmacol Rev 2004;56(4):549–80.
[129] Pepper M, Ferrara N, Orci L, Montesano R. Potent synergism between vascular endothelial growth factor and basic fibroblast growth factor in the induction of angiogenesis *in vitro*. Biochem Biophys Res Commun 1992;189(2):824–31.
[130] Taipale J, Keski-Oja J. Growth factors in the extracellular matrix. FASEB J 1997;11(1):51–9.
[131] Martino MM, Hubbell JA. The 12th–14th type III repeats of fibronectin function as a highly promiscuous growth factor-binding domain. FASEB J 2010;24(12):4711–21.
[132] Martino MM, Briquez PS, Ranga A, Lutolf MP, Hubbell JA. Heparin-binding domain of fibrin (ogen) binds growth factors and promotes tissue repair when incorporated within a synthetic matrix. Proc Natl Acad Sci USA 2013;110(12):4563–8.
[133] De Laporte L, Rice JJ, Tortelli F, Hubbell J. Tenascin C promiscuously binds growth factors via its fifth fibronectin type III-like domain. PLoS ONE 2013;8(4):e62076.
[134] Upton Z, Cuttle L, Noble A, Kempf M, Topping G, Malda J, et al. Vitronectin: growth factor complexes hold potential as a wound therapy approach. J Invest Dermatol 2008;128(6):1535–44.
[135] Liu Y, Cai S, Shu XZ, Shelby J, Prestwich GD. Release of basic fibroblast growth factor from a crosslinked glycosaminoglycan hydrogel promotes wound healing. Wound Rep Reg 2007;15(2):245–51.
[136] Cameron AR, Frith JE, Cooper-White JJ. The influence of substrate creep on mesenchymal stem cell behaviour and phenotype. Biomater 2011;32(26):5979–93.
[137] Cameron AR, Frith JE, Gomez GA, Yap AS, Cooper-White JJ. The effect of time-dependent deformation of viscoelastic hydrogels on myogenic induction and Rac1 activity in mesenchymal stem cells. Biomater 2014;35(6):1857–68.
[138] McKinnon DD, Domaille DW, Cha JN, Anseth K. Biophysically defined and cytocompatible covalently adaptable networks as viscoelastic 3D cell culture systems. Adv Mater 2014;26(6):865–72.
[139] Chaudhuri O, Gu L, Darnell M, Klumpers D, Bencherif SA, Weaver JC, et al. Substrate stress relaxation regulates cell spreading. Nat Comms 2015;6:6365.
[140] Chaudhuri O, Gu L, Klumpers D, Darnell M, Bencherif SA, Weaver JC, et al. Hydrogels with tunable stress relaxation regulate stem cell fate and activity. Nat Mater 2016;15(3):326–34.
[141] Khetan S, Guvendiren M, Legant WR, Cohen DM, Chen CS, Burdick JA. Degradation-mediated cellular traction directs stem cell fate in covalently crosslinked three-dimensional hydrogels. Nat Mater 2013;12(5):458–65.
[142] Zhu W, Qu X, Zhu J, Ma XY, Patel S, Liu J, et al. Direct 3D bioprinting of prevascularized tissue constructs with complex microarchitecture. Biomaterials 2017;124:106–15.
[143] Ozbolat IT, Hospodiuk M. Current advances and future perspectives in extrusion-based bioprinting. Biomaterials 2016;76:321–43.
[144] Vijayavenkataraman S, Yan WC, Lu WF, Wang CH, Fuh JYH. 3D bioprinting of tissues and organs for regenerative medicine. Adv Drug Deliv Rev 2018;132:296–332.
[145] Fedorovich NE, Swennen I, Girones J, Moroni L, van Blitterswijk CA, Schacht E, et al. Evaluation of photocrosslinked lutrol hydrogel for tissue printing applications. Biomacromolecules 2009;10(7):1689–96.
[146] Matricardi P, Pontoriero M, Coviello T, Casadei MA, Alhaique F. *In situ* cross-linkable novel alginate-dextran methacrylate IPN hydrogels for biomedical applications: mechanical characterization and drug delivery properties. Biomacromolecules 2008;9(7):2014–20.
[147] Zhang Y, Yu Y, Akkouch A, Dababneh A, Dolati F, Ozbolat IT. *In vitro* study of directly bioprinted perfusable vasculature conduits. Biomater Sci 2015;3(1):134–43.
[148] Gao Q, He Y, Fu J, Liu A, Ma L. Coaxial nozzle-assisted 3D bioprinting with built-in microchannels for nutrients delivery. Biomaterials 2015;61:203–15.
[149] Gao G, Kim H, Kim BS, Kong JS, Lee JY, Park BW, et al. Tissue-engineering of vascular grafts containing endothelium and smooth-muscle using triple-coaxial cell printing. Appl Phys Rev 2019;6(4):041402.
[150] Andrique L, Recher G, Alessandri K, Pujol N, Feyeux M, Bon P, et al. A model of guided cell self-organization for rapid and spontaneous formation of functional vessels. Sci Adv 2019;5(6):eaau6562.
[151] Cui H, Zhu W, Huang Y, Liu C, Yu ZX, Nowicki M, et al. *In vitro* and *in vivo* evaluation of 3D bioprinted small-diameter vasculature with smooth muscle and endothelium. Biofabrication 2020;12(1):015004.
[152] Saunders RE, Gough JE, Derby B. Delivery of human fibroblast cells by piezoelectric drop-on-demand inkjet printing. Biomaterials 2008;29(2):193–203.
[153] Norotte C, Marga FS, Niklason LE, Forgacs G. Scaffold-free vascular tissue engineering using bioprinting. Biomaterials 2009;30(30):5910–7.
[154] Xu C, Chai W, Huang Y, Markwald RR. Scaffold-free inkjet printing of three-dimensional zigzag cellular tubes. Biotechnol Bioeng 2012;109(12):3152–60.
[155] Cui X, Boland T. Human microvasculature fabrication using thermal inkjet printing technology. Biomaterials 2009;30(31):6221–7.
[156] Guillemot F, Souquet A, Catros S, Guillotin B. Laser-assisted cell printing: principle, physical parameters versus cell fate and perspectives in tissue engineering. Nanomedicine 2010;5(3):507–15.
[157] Wu PK, Ringeisen BR. Development of human umbilical vein endothelial cell (HUVEC) and human umbilical vein smooth muscle cell (HUVSMC) branch/stem structures on hydrogel layers via biological laser printing (BioLP). Biofabrication 2010;2(1):014111.
[158] Cha C, Soman P, Zhu W, Nikkhah M, Camci-Unal G, Chen S, et al. Structural reinforcement of cell-laden hydrogels with microfabricated three dimensional scaffolds. Biomater Sci 2014;2(5):703–9.
[159] Han LH, Suri S, Schmidt CE, Chen S. Fabrication of three-dimensional scaffolds for heterogeneous tissue engineering. Biomed Microdevices 2010;12(4):721–5.
[160] Bertassoni LE, Cardoso JC, Manoharan V, Cristino AL, Bhise NS, Araujo WA, et al. Direct-write bioprinting of cell-laden methacrylated gelatin hydrogels. Biofabrication 2014;6(2):024105.
[161] Kolesky DB, Truby RL, Gladman AS, Busbee TA, Homan KA, Lewis JA. 3D bioprinting of vascularized, heterogeneous cell-laden tissue constructs. Adv Mater 2014;26(19):3124–30.
[162] Miller JS, Stevens KR, Yang MT, Baker BM, Nguyen DHT, Cohen DM, et al. Rapid casting of patterned vascular networks for perfusable engineered three-dimensional tissues. Nat Mater 2012;11(9):768–74.

[163] Mirabella T, MacArthur JW, Cheng D, Ozaki C, Woo YJ, Yang MT, et al. 3D-printed vascular networks direct therapeutic angiogenesis in ischaemia. Nat Biomed Eng 2017;1(6):0083.

[164] Lee VK, Lanzi AM, Ngo H, Yoo SS, Vincent PA, Dai G. Generation of multi-scale vascular network system within 3D hydrogel using 3D bio-printing technology. Cell Mol Bioeng 2014;7(3):460–72.